www.czasopisma.pan.pl PAN POLSKA AKADEMIA NAUK www.journals.pan.pl

Arch. Metall. Mater. **66** (2021), 4, 1019-1022

DOI: 10.24425/amm.2021.136417

SEOK-WOO KO[1], HYEONWOO PARK[2], IL YOO[3], HANSOO KIM[2], JOONHO LEE[2*], BYOUNGCHUL HWANG[1*]

IN-SITU OBSERVATION OF HIGH-TEMPERATURE FRACTURE BEHAVIOUR OF 347 STAINLESS STEEL SUBJECTED TO SIMULATED WELDING PROCESS

In-situ study on the high-temperature fracture behaviour of 347 stainless steel was carried out by using a confocal laser scanning microscope (CLSM). The welding microstructures of the 347 stainless steel were simulated by subjecting the steel specimen to solution and aging treatments. Undissolved NbC carbides were present within grains after solution treatment, and $M_{23}C_6$ carbides were preferentially formed at grain boundaries after subsequent aging treatment. The $M_{23}C_6$ carbides formed at grain boundaries worked as stress concentration sites and thus generated larger cracks during high-temperature tensile testing. In addition, grain boundary embrittlement was found to be a dominant mechanism for the high-temperature fracture of the 347 stainless steel because vacancy diffusion in the Cr-depleted zones enhances intergranular fracture due to the precipitation of $M_{23}C_6$ carbides at grain boundaries.

Keywords: 347 stainless steel, in-situ, high temperature, fracture behaviour, welding, confocal laser scanning microscope (CLSM)

1. Introduction

The 347 stainless steel has been widely used for boiler tubes and pipelines in oil refineries and petrochemical plants because it has excellent high-temperature properties and economic efficiency [1-3]. When the 347 stainless steel is exposed to the service temperature of 400~650°C for a long time, fine and coarse carbides can be formed within grains or at the grain boundaries [4,5]. On the other hand, the precipitation of Cr-rich carbides at the grain boundaries creates a Cr-depleted zone in the 347 stainless steel. As a result, the Cr-depleted zone increases vacancy diffusion at the grain boundaries, and thus promotes intergranular fracture [6]. In addition, the presence of coarse carbides such as $M_{23}C_6$ carbides at the grain boundary would act as stress concentration sites and thus initiate fracture under load [7,8].

In this study, two kinds of 347 stainless steel specimens with different heat treatment conditions were prepared in order to investigate the effect of the $M_{23}C_6$ carbide on the high-temperature tensile and fracture behaviour. In particular, the crack initiation and propagation of the 347 stainless steel specimens were examined during high-temperature tensile test via confocal laser scanning microscope (CLSM).

2. Experimental

The 347 stainless steel with a chemical composition of Fe-17Cr-9Ni-0.82Mn-0.42Nb-0.35Si-0.04C (wt. %) was used for this study. To simulate the precipitation-free zone at grain boundary in the HAZ of the 347 stainless steel, the specimen was subjected to solution treatment at 1,150°C for 2 h, followed by water quenching. After the solution treatment, subsequent aging treatment was additionally performed at 600°C for 20 h in order to precipitate $M_{23}C_6$ carbides which can be formed during the actual operating temperature of the 347 stainless steel. For convenience, they were referred to as 'solution-treated' and 'aging-treated' according to the heat treatment condition. After the specimens were mechanically polished and etched by using aqua regia (15 ml HCl + 5 ml HNO_3), the corresponding microstructures were observed by a high-resolution SEM (HR-SEM, SU8010, Hitachi, Japan).

According to ASTM E8 standard test method, sub size sheet-type tensile specimens with a gage width of 6.3 mm and a gage length of 25.0 mm were prepared and were tested at room temperature and strain rate of 1×10^{-3} s^{-1} using a 10-ton universal testing machine (UT-100E, MTDI, Korea). For high-temperature

[1] SEOUL NATIONAL UNIVERSITY OF SCIENCE AND TECHNOLOGY, DEPARTMENT OF MATERIALS SCIENCE AND ENGINEERING, 232 GONGNEUNG-RO, NOWON-GU, SEOUL 01811, REPUBLIC OF KOREA
[2] KOREA UNIVERSITY, DEPARTMENT OF MATERIALS SCIENCE AND ENGINEERING, SEOUL 02841, REPUBLIC OF KOREA
[3] ADNOC LNG, ABU DHABI, UNITED ARAB EMIRATES

* Corresponding authors: bhwang@seoultech.ac.kr; joonholee@korea.ac.kr

tensile test and in-situ observation, tensile test was performed on the specimens with a gage width 5.0 mm and a gage length of 25.0 mm at the temperature of 800°C and the strain rate of 1×10^{-3} s^{-1} using a 500-kgf high-temperature tension and compression equipment (VL2000DX, Yonekura, Japan) and CLSM. In order to prevent surface oxidation during the test, the surface of the specimen was coated with platinum, which does not react with oxygen. In addition, reducing hydrogen and helium gas was injected into the chamber to remove oxygen from the chamber to prevent oxidation.

3. Results and discussion

The SEM images of the solution- and aging-treated specimens for the 347 stainless steel are shown in Fig. 1(a)-(d), and the corresponding EDS analysis results of the precipitates are provided next to the SEM images. In the 347 stainless steel specimens composed of fully austenite single phase, undissolved primary NbC carbides were observed within the grains after solution treatment (Fig. 1(a)-(b)) [9]. On the other hand, additional precipitates were formed in the grains and at the grain boundaries after aging treatment. It is well-known that the segregation and precipitation occurred preferentially at grain boundaries owing to the high energy of the grain boundary. Therefore, fine secondary NbC carbides were precipitated within the grains, whereas $M_{23}C_6$ carbides were formed mostly at the grain boundaries (Fig. 1(c)-(d)) [10,11].

Fig. 2 presents the room-temperature and high-temperature engineering stress-strain curves of the 347 stainless steel. The aging-treated specimen had a higher strength and lower elongation than the solution-treated specimen. The higher strength of the aging-treated specimen results from the precipitation hardening of fine secondary NbC carbides. The $M_{23}C_6$ carbides at the grain boundaries would act as stress concentration sites and thus lead to the lower elongation of the aging-treated specimen [12,13]. High-temperature tensile test results revealed that all the specimens exhibited lower tensile strength and lower elongation at high temperatures than at room temperature, probably due to the easiness of dislocation climb and grain boundary embrittlement at high temperatures [14]. The elongation of the aging-treated specimen at high temperatures was 10% lower than that of the solution-treated specimen. Langdon et al. reported that the increase of vacancy diffusion in the Cr-depleted zone encourages

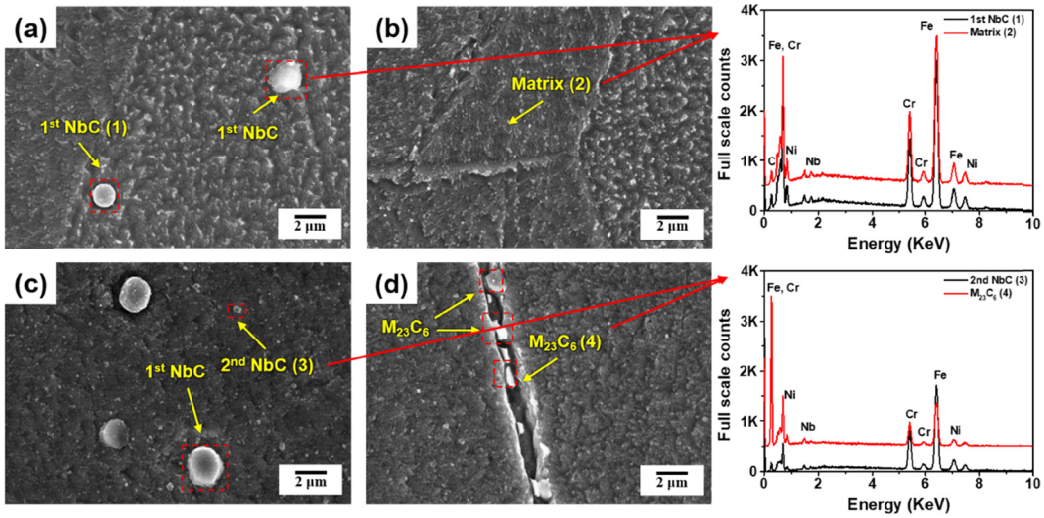

Fig. 1. SEM images and EDS analysis results of the (a) grain interior and (b) grain boundary of the solution-treated specimen, and the (c) grain interior and (d) grain boundary of the aging-treated specimen for the 347 stainless steel

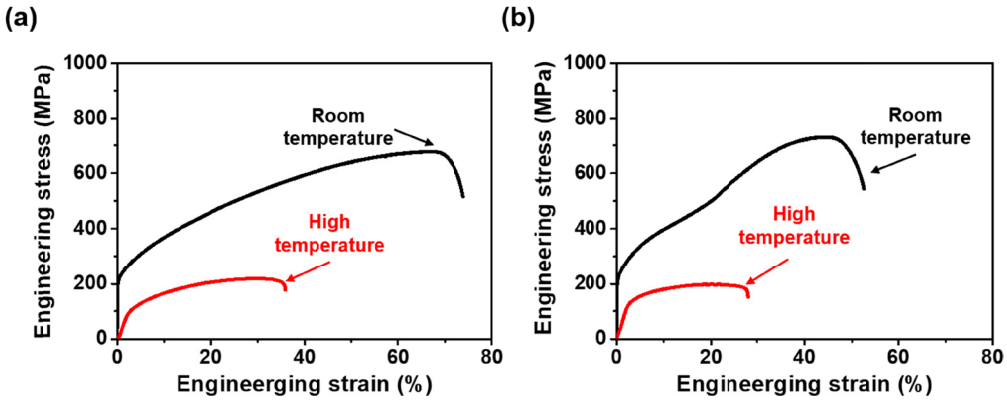

Fig. 2. Engineering stress-strain curves of the (a) solution- and (b) aging-treated specimens. Tensile tests were conducted at room temperature and high temperature (800°C) for the 347 stainless steel

grain boundary sliding [15]. Therefore, the formation of $M_{23}C_6$ carbides at the grain boundaries could cause Cr-depleted zones, and thereby leads to the lower elongation of the aging-treated specimen.

The high-temperature fracture behaviour of the 347 stainless steel was examined by in-situ CLSM, and the corresponding images are given in Figs. 3 and 4. The initial microstructure of the solution-treated specimen when the load was 0 N is shown in Fig. 3(a). With an increase in the load to 200 N, slip bands were formed, and the shape of the slip band was clearly observed with an increase in the load (Fig. 3(b)-(c)). When the load was increased to 600 N, microcracks perpendicular to the tensile direction were initiated at the grain boundary. As the load increased, the initiation and propagation of microcracks at the grain boundary increased. Finally, the cracks propagated along the grain boundary, and fracture occurred (Fig. 3(d)-(f)).

Similarly, in the aging-treated specimen, slip bands appeared with an increase in as the load from 0 N, and microcracks were initiated and propagated when the load was above 600 N (Fig. 4(a)-(d)). However, with a further increase in the from 800 N, the aging-treated specimen exhibited a larger crack and the crack propagated more rapidly (Fig. 4(e)-(f)). The $M_{23}C_6$ carbides precipitated at the grain boundaries can be generated Cr-depleted zones which increased vacancy diffusion at grain

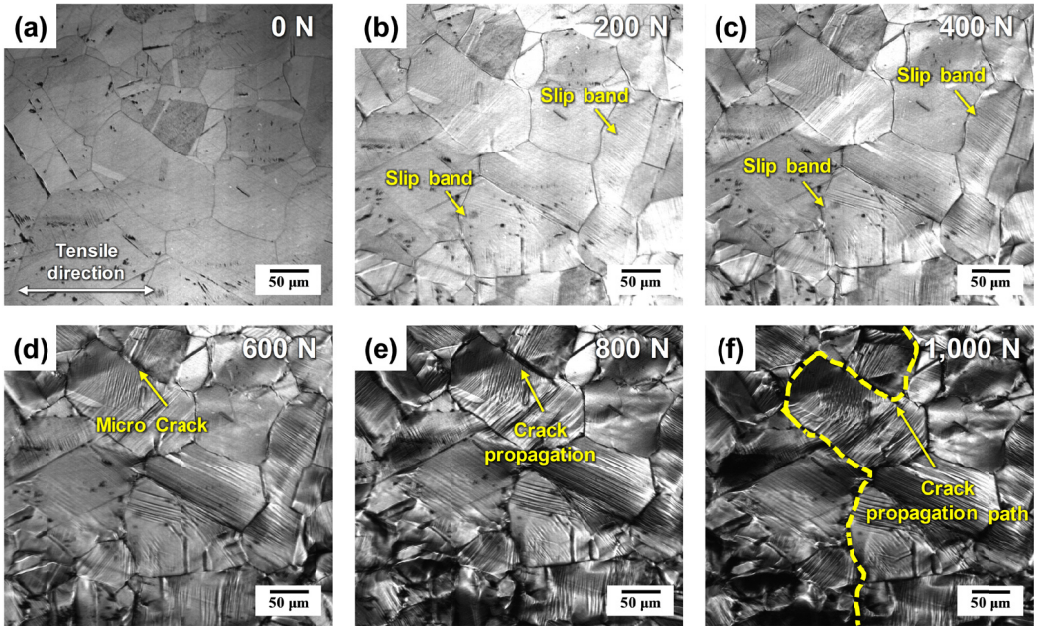

Fig. 3. CLSM images of the solution-treated specimen tested at the temperature of 800°C in the load conditions of the (a) 0 N, (b) 200 N, (c) 400 N, (d) 600 N, (e) 800 N and (f) 1,000 N, showing the formation of slip band, micro-crack initiation and propagation of the 347 stainless steel

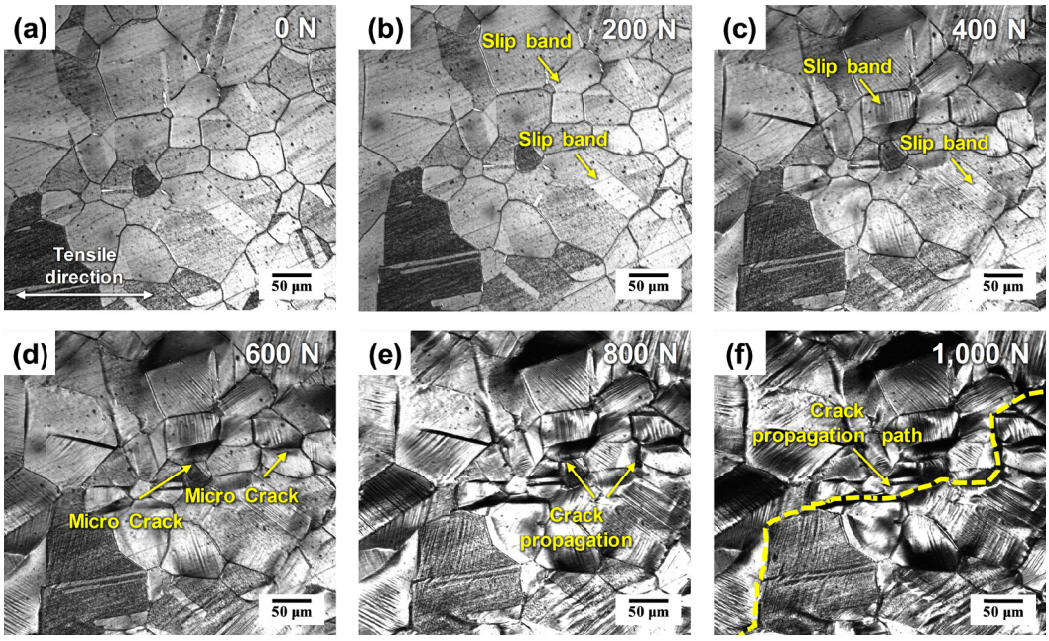

Fig. 4. CLSM images of the aging-treated specimen tested at the temperature of 800°C in the load conditions of the (a) 0 N, (b) 200 N, (c) 400 N, (d) 600 N, (e) 800 N and (f) 1,000 N, showing the formation of slip band, micro-crack initiation and propagation of the 347 stainless steel

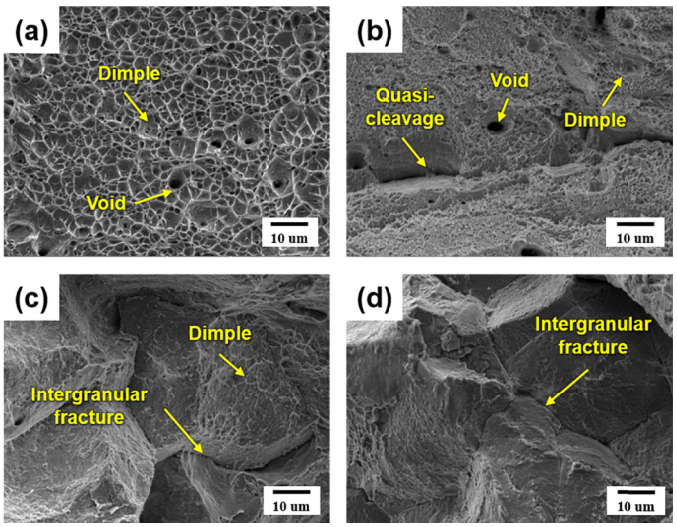

Fig. 5. SEM fractographs of the (a) solution- and (b) aging-treated specimens tested at room temperature, and the (c) solution- and (d) aging-treated specimens tested at the temperature of 800°C

boundaries and enhanced intergranular fracture [16]. As a result, $M_{23}C_6$ carbides acted as stress concentration sites and grain boundary embrittlement occurred easily [17,18].

Fig. 5 provides the SEM fractographs of the specimens tested at room and high temperatures. The solution-treated specimen exhibited mostly ductile fracture, where large dimples were observed particularly at room temperature. In aging-treated specimen, quasi-cleavage fractures were often observed owing to the formation of $M_{23}C_6$ carbides at grain boundaries and fine dimples were found near the quasi-cleavage fracture. Intergranular fractures were mainly observed in the solution- and aging-treated specimens tested at high temperatures.

4. Conclusions

In this study, the high-temperature tensile properties and fracture behaviour of the 347 stainless steel were investigated and the following conclusions were drawn:

1. For the 347 stainless steels, the SEM and EDS analysis results revealed that $M_{23}C_6$ carbides were additionally precipitated at the grain boundaries after subsequent aging treatment, while maintaining undissolved NbC carbides within grains after solution treatment.
2. The aging-treated specimen had a higher tensile strength and lower elongation than the solution-treated specimen because fine NbC carbides within grains contributed to precipitation hardening and $M_{23}C_6$ carbides formed at grain boundaries acted as stress concentration sites in the aging-treated specimen.
3. In-situ observation of the high-temperature fracture behaviour of the 347 stainless steel showed that slip bands were distinctly formed throughout the grains and microcracks began to initiate at the grain boundaries beyond a certain load. Particularly, the initiation and propagation of some cracks occurred more actively in the aging-treated specimen.
4. Grain boundary embrittlement was found to be a dominant mechanism for the high-temperature deformation and fracture behaviour of the 347 stainless steel because vacancy diffusion in the Cr-depleted zones enhances intergranular fracture due to the precipitation of $M_{23}C_6$ carbides at grain boundaries.

Acknowledgments

This study was supported by the Research Program funded by the SeoulTech (Seoul National University of Science and Technology)

REFERENCES

[1] N. Kim, W. Gil, H. Lim, C. Choi, H. Lee, Met. Mater. Int. **25**, 193-206 (2019).
[2] B. Jian, X. Hu, Y. Liu, Mat. Mater. Int. **26**, 1295-1305 (2020).
[3] H.P. Kim, D.J. Kim, Corros. Sci. Tech. **17**, 183-192 (2018).
[4] Y. Zhou, Y. Li, Y. Liu, Q. Guo, C. Liu, L. Yu, C. Li, H. Li, J. Mater. Res. **30**, 3642-3652 (2015).
[5] B. Sasmal, J. Mater. Sci. **32**, 5439-5444 (1997).
[6] K. Kaneko, T. Fukunage, K. Yamada, N. Nakada, M. Kikuchi, Z. Saghi, J.S. Barnard, P. A. Midgley, Scr. Mater. **65**, 509-512 (2011).
[7] J. Vivas, C. Capdevila, E. Altstadt, M. Houska, I. Sabirov, D.S. Mart, Met. Mater. Int. **25**, 343-352 (2019).
[8] H.U. Hong, B.S. Rho, S.W. Nam, J. Mater. Sci. Eng. A. **318**, 285-292 (2001).
[9] S.G. Kim, J.N. Kim, J.P. Wang, C.Y. Kang, Met. Mater. Int. **25**, 127-134 (2019).
[10] J.P. Adamson, J.W. Martin, Acta Mater. **19**, 1015-1018 (1971)
[11] S.H. Lee, H.S. Na, K.W. Lee, Y. Choe, C.Y. Kang, Metals. **8**, 1-14 (2018)..
[12] Y.M. He, Y.H. Wang, K. Guo, T.S. Wang, J. Mater. Sci. Eng. A. **708**, 248-253 (2017).
[13] S.I. Lee, S.Y. Lee, J. Han, B. Hwang, Mater. Sci. Eng. A. **742**, 334-343 (2019).
[14] R. Raj, M.F. Ashby, Metall. Mater. Trans. **2**, 1113-1127 (1971).
[15] T.G. Langdon, Acta Metal. Mater. **42**, 2437-2443 (1994).
[16] Q. Wu, T. Han, Y. Wang, H. Wang, H. Zhang, S. Gu, Eng. Fail. Anal. **109**, 104236 (2020).
[17] E. Merson, V. Danilov, D. Merson, A. Vinogradov, Eng. Fract. Mech. **183**, 147-158 (2017).
[18] J. Tian, G. Xu, X. Wan, Mat. Mater. Int. **26**, 961-972 (2020).
[19] S.I. Lee, S.Y. Lee, S.G. Lee, H.G. Jung, B. Hwang, Met. Mater. Int. **24**, 1221-1231 (2018).
[20] S.Y. Lee, S.I. Lee, B. Hwang, Mater. Sci. Eng. A. **711**, 22-28 (2018).
[21] S.I. Lee, J. Lee, B. Hwang, Mater. Sci. Eng. A. **758**, 56-59 (2019).